The EMBO Journal (2006) 25, 4628–4637 | © 2006 European Molecular Biology Organization | All Rights Reserved 0261-4189/06
www.embojournal.org

THE EMBO JOURNAL

A streptococcal protease that degrades CXC chemokines and impairs bacterial clearance from infected tissues

Carlos Hidalgo-Grass[1,4], Inbal Mishalian[1,4], Mary Dan-Goor[1], Ilia Belotserkovsky[1], Yoni Eran[1], Victor Nizet[2], Amnon Peled[3] and Emanuel Hanski[1,*]

[1]Institute of Microbiology, The Hebrew University-Hadassah Medical School, Jerusalem, Israel, [2]Department of Pediatrics, School of Medicine, University of California, San Diego, La Jolla, CA, USA and [3]Goldyne Savad Institute of Gene Therapy, Hadassah University Hospital, Jerusalem, Israel

Group A *Streptococcus* (GAS) causes the life-threatening infection in humans known as necrotizing fasciitis (NF). Infected subcutaneous tissues from an NF patient and mice challenged with the same GAS strain possessed high bacterial loads but a striking paucity of infiltrating polymorphonuclear leukocytes (PMNs). Impaired PMN recruitment was attributed to degradation of the chemokine IL-8 by a GAS serine peptidase. Here, we use bioinformatics approach coupled with target mutagenesis to identify this peptidase as ScpC. We show that SilCR pheromone downregulates *scpC* transcription via the two-component system—SilA/B. In addition, we demonstrate that *in vitro*, ScpC degrades the CXC chemokines: IL-8 (human), KC, and MIP-2 (both murine). Furthermore, using a murine model of human NF, we demonstrate that ScpC, but not the C5a peptidase ScpA, is an essential virulence factor. An ScpC-deficient mutant is innocuous for untreated mice but lethal for PMN-depleted mice. ScpC degrades KC and MIP-2 locally in the infected skin tissues, inhibiting PMN recruitment. In conclusion, ScpC represents a novel GAS virulence factor functioning to directly inactivate a key element of the host innate immune response.

The EMBO Journal (2006) **25,** 4628–4637. doi:10.1038/sj.emboj.7601327; Published online 14 September 2006
Subject Categories: immunology; microbiology & pathogens
Keywords: chemokines; group A *Streptococcus*; peptidase; polymorphonuclear neutrophils; virulence

Introduction

Group A *Streptococcus* (GAS, *Streptococcus pyogenes*) is a major Gram-positive bacterial pathogen associated with a wide spectrum of human diseases, ranging from superficial throat and skin infections to life-threatening invasive conditions such as necrotizing fasciitis (NF) (Cunningham, 2000; Bisno *et al*, 2003). NF is an infection that results in a rapid and progressive destruction of fascia and fat (Kaul *et al*, 1997) that is frequently complicated by development of toxic shock syndrome (TSS). Even with prompt antibiotic treatment and surgical debridement, reported mortality rates in GAS NF and TSS are high, ranging from 20 to 60% (Davies *et al*, 1996; Kaul *et al*, 1997; Hassell *et al*, 2004). Although NF can be produced by GAS of various serotypes (Johnson *et al*, 2002; Bisno *et al*, 2003; Hassell *et al*, 2004), M1 and M3 strains have been most commonly reported (Cleary *et al*, 1992; Monnickendam *et al*, 1997; O'Brien *et al*, 2002; Sharkawy *et al*, 2002). Our prospective, population-based study of invasive GAS infections in Israel further identified M14 strains as strongly associated with severe soft tissue infections (Moses *et al*, 2003).

In vivo screening of a transposon-tagged mutant library from an invasive M14 GAS isolate identified the streptococcal invasion locus (*sil*) as essential for rapid dissemination of GAS in a murine model of NF (Hidalgo-Grass *et al*, 2002). GAS *sil* shares homology with the genetic competence regulon of *Streptococcus pneumoniae* (Claverys and Havarstein, 2002). It includes the two-component system (TCS) SilA/B and the ABC-type transporter SilD/E. Situated between these entities and preceded by a combox-like promoter (Morrison and Lee, 2000) lies the small open reading frame (ORF) *silC*. Highly overlapping *silC*, but transcribed from the reverse strand, is a sixth ORF SilCR, which is a putative competence stimulating peptide (CSP).

In the M14 serotype strains, a start codon mutation eliminates expression of the putative CSP SilCR (Hidalgo-Grass *et al*, 2002). We have hypothesized that *sil*, and SilCR in particular, may function to negatively regulate the invasive disease potential of GAS. Support for this hypothesis was provided in experiments in which mice were challenged with M14 GAS JS95 wild-type (WT) strain with or without simultaneous injection of the mature synthetic SilCR peptide. Compared to mice challenged with WT alone, co-administration of SilCR dramatically reduced bacterial proliferation, tissue necrosis, and mortality (Hidalgo-Grass *et al*, 2004). In mice inoculated with the WT alone, we observed a rapid spread of bacteria into the necrotic soft tissues in conjunction with a striking paucity of polymorphonuclear leukocyte (PMN) infiltration. Administration of SilCR altered the equation, triggering PMN recruitment to the site of infection with restriction of infectious spread (Hidalgo-Grass *et al*, 2004). The observation that a culture medium of the WT strain degrades *in vitro* the CXC chemokine IL-8, but when grown in the presence of the SilCR peptide IL-8 degradation is lost (Hidalgo-Grass *et al*, 2004), offers a potential mechanism for this effect.

In the present study, we apply a bioinformatics analysis and real-time RT–PCR measurement coupled with targeted

*Corresponding author. Faculty of medicine, Institute of Microbiology, The Hebrew University-Hadassah Medical School, Jerusalem 91010, Israel. Tel.: +972 2 6758196; Fax: +972 2 6434170;
E-mail: hanski@cc.huji.ac.il
[4]These authors contributed equally to this work

Received: 19 May 2006; accepted: 16 August 2006; published online: 14 September 2006

mutagenesis to identify ScpC as the protease responsible for IL-8 degradation. We show that ScpC degrades the murine CXC chemokines KC and MIP-2 *in vitro* and in the tissues of experimentally infected mice, thereby critically impairing the PMN innate immune response.

Results

Identification of GAS serine proteases transcriptionally repressed by SilCR

We hypothesized that SilCR may reduce IL-8 degradation by repressing the transcription of the gene encoding the GAS IL-8 peptidase. To identify possible gene candidates for such a peptidase, we used the MEROPS database http://merops.sanger.ac.uk (Rawlings *et al*, 2004), which classified the GAS serine peptidases into 12 families. Excluding those groups associated with basic cellular maintenance functions, we concentrated on five families S1C, S8A, S9C, S15, and S54 (description of the families of these peptidases and their possible roles in virulence and chemokine degradation is detailed in Supplementary data).

Transcription of each serine peptidase gene in the WT was determined in the presence or absence of SilCR using real-time RT–PCR (Figure 1A), with primers designed to amplify any GAS allele belonging to the indicated families (Supplementary Table I). Of the entire candidate peptidase genes tested, only the transcription of SPy0416 (which we termed ScpC; see below) was significantly affected by SilCR administration, with a 10-fold reduction in mRNA levels. This result suggested that the SPy0416 could represent the serine peptidase activity, under negative regulation of SilCR, which functions to promote GAS chemokine degradation. Indeed, a mutant defective in SilA (*silA*), the response regulator of the TCS of the *sil* locus, had a 10-fold lower transcription of the protease than the WT and lost completely the ability to degrade IL-8 *in vitro* (Supplementary Figure 1S).

Coupled with the knowledge of the recent description of IL-8 degradation by a partially purified cell-envelope peptidase (CEP) preparation SpyCEP (Edwards *et al*, 2005). We were encouraged to pursue molecular genetic studies to establish the contribution of the protease to disease pathogenesis. There are several different CEPs in GAS, and SpyCEP has an extensive homology to the C5a peptidase ScpA. To conform more closely to standard GAS gene nomenclature, we elected therefore to call this gene and encoded peptidase *scp*C and ScpC, respectively (for streptococcal chemokine protease).

Analysis of ScpC domains

The GAS gene encoding ScpC resides between a gene encoding lactate oxidase (*lct*O) and an ORF of unknown function (Spy0421) (Figure 1B). By homology inference to other subtilisin-like serine CEPs (Siezen, 1999) (detailed in Supplementary data), we found that ScpC is composed of six putative domains: (PP) the pre-pro domain, which begins with a signal sequence; (PR) the peptidase domain, which contains the candidate catalytic triad of Asp + His + Ser; (A) and (B/H) domains, potentially serving as spacers for proper positioning of the active site; (W) and (AN), cell wall-anchoring domains that are separated by the LPxTG motif (Ton-That *et al*, 2004) (Figure 1B). The *scpC* gene is present in all 12 available GAS genomes encoding proteins that are highly homologous (87.8% amino-acid (aa) identity, 99.6% aa similarity).

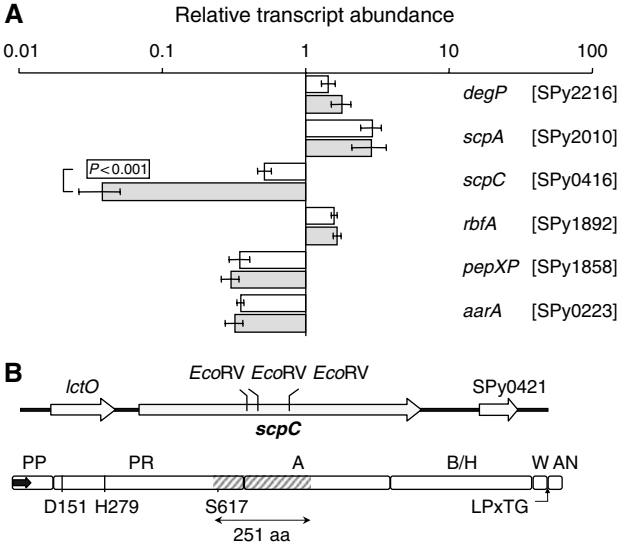

Figure 1 Identification of ScpC as a putative IL-8 protease. (**A**) The effect of SilCR on the transcription of GAS serine peptidase. The abundance of the indicated serine peptidase transcripts relative to that of *gyrA* was determined by real-time RT–PCR in RNA derived from WT grown to OD of 0.4 at 600 nm in the absence (clear bars) or presence (shaded bars) of SilCR (10 μg/ml). The values are mean obtained from analysis in duplicate of three independent RNA samples. Error bars represent standard deviation (s.d.). SilCR down-regulates the transcription of *scpC*. $P<0.001$ (Student's test). (**B**) Genomic arrangement and domain organization of ScpC. Upper panel: The arrows depict the identified ORFs and their direction of transcription. The 5′ and 3′ *Eco*RV sites at positions 1801 and 2554 bp from the beginning of *scpC* were used to replace the internal *scpA* coding sequence with Ω*km2*. *spy0421* encodes a product of 236 aa with no homology to characterized proteins. Lower panel: The map of the motifs identified in the predicted sequence of ScpC includes the following: the pre-pro (PP) domain (residues 1–123) containing the signal sequence (residues 1–34) depicted as an arrow, protease domain (PR) (residues 124–688) containing Asp, His, and Ser forming the catalytic triad; the A domain (residues 689–1128) and the B/H domain (residues 1129–1560), the cell wall domain (W) (residues 1561–1613), the cell wall anchor domain (AN) (residues 1613–1647), and the LPxTG motif starting at residue 1613. The DNA region removed by the *Eco*RV digestion contains a segment of 251 aa (hatched) including Ser617 of the catalytic triad.

Construction of ScpA- and ScpC-deficient mutants and assessment of their role in virulence

ScpA and ScpC prevent adequate recruitment and activation of PMN *in vitro* (DeMaster *et al*, 2002; Edwards *et al*, 2005); thus, the two peptidases might have overlapping roles in GAS pathogenesis. To test the contribution to virulence of ScpC in the absence of ScpA, we first constructed a Δ*scpA* mutant in the WT M14 GAS strain. The Δ*scpA* mutant was obtained by replacing 2752 bp from the coding region of the gene with *aad9* (Supplementary Tables I and II). Loss of ScpA expression in the mutant was confirmed by dot blot analysis (Supplementary Figure 2S). Secondly, we deleted *scpC* in the *scpA*-deficient background. The Δ*scpA*/Δ*scpC* double mutant was constructed by replacing a 753 bp internal *Eco*RV fragment of *scpC* coding region (Figure 1B), including the critical serine residue of the catalytic triad with Ω-*Km2* element. The fidelity of *scpC* replacement was confirmed as detailed in Materials and methods.

The WT GAS parental strain and its isogenic Δ*scpA* and Δ*scpA*/Δ*scpC* mutants demonstrated equivalent logarithmic growth in Todd–Hewitt Yeast (THY) media (Supplementary Figure 3Sa) and similar proliferation rates in nonimmune whole human blood (Supplementary Figure 3Sb). This result indicates that neither of the peptidases contributes significantly to GAS whole blood survival. As surface-expressed M and M-like proteins are absolutely required for GAS resistance to phagocytic killing by complement and non-stimulated PMNs (Bisno *et al*, 2003), these results also imply that both Δ*scpA* and Δ*scpA*/Δ*scpC* mutants maintain adequate levels of M protein expression. Despite different strategies used and several attempts, we were unable to inactivate *scpC* without first inactivating *scpA* (for details see Supplementary Figure 4S). This may imply that there could be a functional linkage between ScpA and ScpC in the M14 strain containing the *sil* locus.

Next, we tested the relative contribution of ScpA and ScpC to virulence in a murine model of GAS NF. All mice challenged with either the WT or the Δ*scpA* mutant experienced a rapidly progressing infection and death between 2 and 7 days after challenge (Figure 2A). The Kaplan–Meier analysis showed that the rates of death of mice inoculated with the WT and the Δ*scpA* mutant were similar. In marked contrast, only three mice out of the 28 challenged with the Δ*scpA*/Δ*scpC* mutant succumbed to the infection (Figure 2A), proving it to be significantly less virulent than either the WT or the Δ*scpA* mutant. As shown, weight changes paralleled the data shown in Figure 2A. Mice challenged with WT and the Δ*scpA* mutant showed progressive weight loss before death, whereas mice challenged with the Δ*scpA*/Δ*scpC* mutant regained weight by day 2 with progressive weight gain thereafter (Figure 2B). Mice challenged with either the WT or the Δ*scpA* mutant developed visible necrotic skin lesions of similar size 1 day after the inoculation (Figure 2C). At day 2 after inoculation, the lesion size of the WT and the Δ*scpA* mutant expanded and continued to increase in size until mice died by day 4 after the infection. In contrast, mice challenged with the Δ*scpA*/Δ*scpC* double mutant developed small lesions peaking in size on day 2 (Figure 2C), followed by slow resolution and complete healing by day 14 (not shown). Grossly, the small lesions caused by Δ*scpA*/Δ*scpC* mutant were superficial in nature, whereas the lesions produced by either the WT GAS or the Δ*scpA* mutant were deeper and more necrotic.

In vitro degradation of chemokines by ScpC

To provide direct evidence that ScpC was responsible for chemokine degradation, we tested the set of the isogenic mutants using an *in vitro* IL-8 degradation assay. The Δ*scpA* mutant degraded IL-8 as efficiently as the parental WT strain (Figure 3A). In contrast, the isogenic Δ*scpA*/Δ*scpC* double

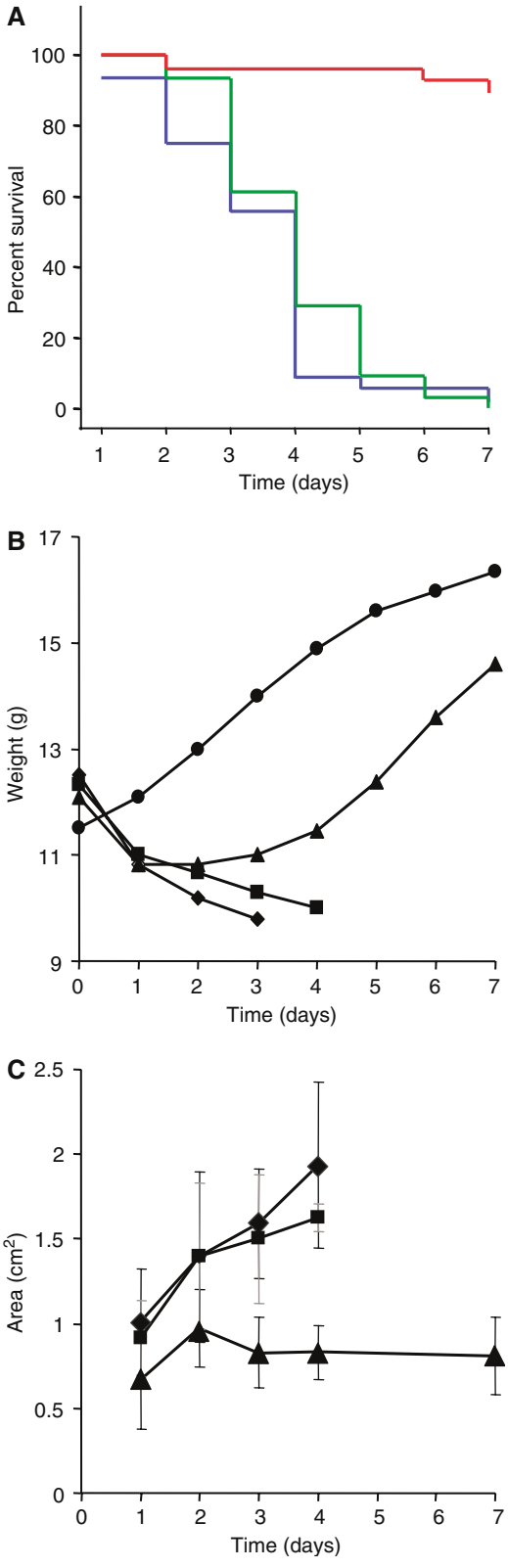

Figure 2 ScpC significantly contributes to virulence in the murine model of GAS necrotizing soft tissue infections. (**A**) Inactivation of *scpC* but not of *scpA* abolished lethality of GAS. Mice were injected subcutaneously with 1×10^8 CFU of WT (— $n=32$), Δ*scpA* (— $n=31$), and Δ*scpA*/Δ*scpC* (— $n=28$) and survival was monitored daily. The Kaplan–Meier analysis performed on five different experiments shows $P<0.001$ for Δ*scpA*/Δ*scpC* versus WT or versus Δ*scpA* and $P>0.05$ for WT versus Δ*scpA* (log rank (Mantel–Cox) test). (**B**) Weight change in control mice (●) and mice challenged with 1×10^8 CFU of WT (◆), Δ*scpA* (■), and Δ*scpA*/Δ*scpC* (▲). Experiments were repeated five times with similar results. (**C**) Mean total lesion size (cm^2). Mice were injected with 1×10^8 CFU of WT (◆ $n=9$), Δ*scpA* (■ $n=15$), and Δ*scpA*/Δ*scpC* (▲ $n=9$), photographed daily, and the area was calculated using ImageJ software. Error bars represent s.d. WT and Δ*scpA* versus Δ*scpA*/Δ*scpC* $P<0.05$ (Student's test) for time points 1 and 2 and $P<0.001$ (Student's test) for time points 3 and 4. WT versus Δ*scpA* $P>0.05$ (Student's test) at all time points.

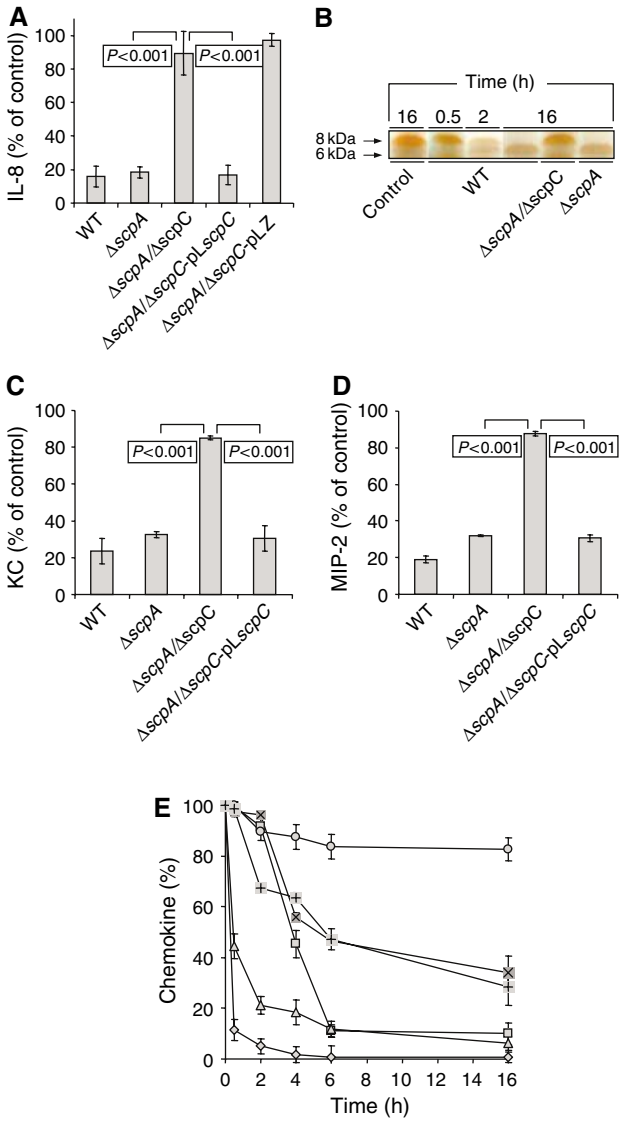

Figure 3 ScpC is absolutely required for chemokine degradation. (**A**) ScpC is responsible for IL-8 degradation. The determination of IL-8 after 2 h of proteolysis in control (in the absence of bacterial supernatant, 100%) and in supernatants of WT, Δ*scpA*, Δ*scpA*/Δ*scpC*, Δ*scpA*/Δ*scpC*-pL*scpC*, and Δ*scpA*/Δ*scpC*-pLZ was conducted by ELISA. The values are the mean obtained from analysis in duplicate ($n=3$). Error bars represent s.d. (**B**) IL-8 is cleaved by WT supernatant. Control represents IL-8 incubated for 16 h in the absence of bacterial supernatant. Samples containing IL-8 and supernatants from WT, Δ*scpA*/Δ*scpC*, and Δ*scpA* were incubated for the indicated time points and subjected to 17.5% SDS–PAGE, which was then silver stained. The arrows represent the molecular weights of IL-8 and of the generated 6 kDa form. (**C**) ScpC is responsible for KC degradation. The determination of KC after 16 h of proteolysis in control (in the absence of bacterial supernatant, 100%) and supernatants of WT, Δ*scpA*, Δ*scpA*/Δ*scpC*, and Δ*scpA*/Δ*scpC*-pLScpC was conducted by ELISA. The values are the mean obtained from analysis in duplicate ($n=3$). Error bars represent s.d. (**D**) ScpC is responsible for MIP-2 degradation. The determination of MIP-2 after 16 h of proteolysis in control (in the absence of bacterial supernatant, 100%) and supernatants of WT, Δ*scpA*, Δ*scpA*/Δ*scpC*, and Δ*scpA*/Δ*scpC*-pLScpC was conducted by ELISA. The values are mean obtained from analysis in duplicate ($n=3$). Error bars represent s.d. (**E**) Kinetics of chemokine degradation. WT supernatant was incubated with IL-8 (◇), KC (△), MIP-2 (□), RANTES (○), LIX_{74} (⊠), or LIX_{93} (+) and the concentration of the chemokines at the indicated time points was determined by ELISA. 100% represents the concentration of chemokines at time zero. Error bars represent s.d.

mutant showed minimal IL-8-degrading ability (Figure 3A). To further demonstrate that ScpC was specifically responsible for IL-8 degradation, the Δ*scpA*/Δ*scpC* mutant was transformed with the expression vector pLZ (Husmann *et al*, 1995) harboring a full copy of the *scpC* gene (pL*scpC*; Supplementary Table II). Whereas the Δ*scpA*/Δ*scpC* mutant complemented with the vector alone (pLZ) did not degrade IL-8, the Δ*scpA*/Δ*scpC* mutant complemented with pL*scpC* demonstrated full restoration of IL-8 proteolysis (Figure 3A). These results indicate that ScpC but not ScpA is required for IL-8 degradation.

In experiments reported by Edwards *et al* (2005) GAS cleave IL-8 at the C-terminus between Glu59 and Arg60 to generate peptides of ~6 and ~2 kDa, the former of which could be clearly identified on 17.5% SDS–PAGE (Edwards *et al*, 2005). Elimination of the last 14 aa at the C-terminus of IL-8 is known to markedly impair the chemokines' ability to stimulate PMN chemotaxis (25-fold reduction) and elastase release (50-fold reduction) (Clark-Lewis *et al*, 1991; Edwards *et al*, 2005).

IL-8 proteolysis by WT culture supernatant was followed by SDS–PAGE using a starting concentration of 3.0 μg/ml of the chemokine peptide (Figure 3B). The 6 kDa proteolytic fragment of IL-8 was detected clearly after 2 h and by 16 h all the IL-8 had been cleaved to the 6 kDa form. IL-8 was not degraded by culture supernatant from the Δ*scpA*/Δ*scpC* mutant, yet it was completely processed into the 6 kDa fragment by culture supernatant of the Δ*scpA* mutant (Figure 3B). These data show that ScpC is solely responsible for the secreted IL-8 proteolytic activity of GAS.

KC and MIP-2 are functional murine homologs of IL-8, playing significant roles in both wound healing (Gillitzer and Goebeler, 2001) and the host innate immune responses to Gram-positive bacterial skin infection (Miller *et al*, 2006). In addition, the CXC chemokine murine granulocyte chemotactic protein 2, also termed as LPS-induced CXC chemokine (LIX), was shown to induce PMN infiltration in mice, particularly after N- and C-terminal truncation (Wuyts *et al*, 1999).

Using our isogenic mutants, we found that the WT GAS parental strain and the Δ*scpA* mutant each efficiently degraded KC and MIP-2 (Figure 3C and D). In contrast, the isogenic Δ*scpA*/Δ*scpC* mutant demonstrated a complete loss of KC and MIP-2 degradation (Figure 3C and D), showing that ScpC is solely responsible for the degradation of these murine chemokines. MIP-2 is cleaved at the C-terminus by a partially purified ScpC preparation but less effectively than IL-8 (Edwards *et al*, 2005). To compare the relative rate of CXC chemokine degradation by ScpC, we subjected IL-8, KC, MIP-2, LIX (two forms of the mature peptide stretching from aa 5 to 78 (LIX_{74}) and from aa 1 to 93 (LIX_{93})) and the CC mouse chemokine RANTES to proteolysis by WT supernatant. Comparative analysis of chemokine degradation by WT GAS supernatant revealed that 90% of IL-8 and 60% of KC were degraded within 30 min, whereas MIP-2 degradation was slower but completed after 6 h of incubation. In contrast, the two forms of LIX were only partially degraded, even after prolonged incubation of 16 h. RANTES was not affected at all (Figure 3E). These results demonstrate that the cleavage of CXC chemokines by ScpC is specific and the preferable substrates in a descending order are IL-8, KC, MIP-2, and LIX.

In vivo degradation of chemokines by ScpC and its impact on PMN recruitment

We sought to establish a connection between the ability of ScpC to degrade CXC chemokines *in vitro* (Figure 3), and the clear contribution of ScpC to GAS virulence in the murine model of NF (Figure 2). KC, MIP-2, and LIX protein levels in extracts from skin biopsies taken at 0, 6, 12, 24, and 48 h after inoculation of mice were measured by ELISA. KC levels in the skin of mice infected with Δ*scpA*/Δ*scpC* mutant rose rapidly within 6 h of bacterial challenge, peaking at 15 ng/mg extracted protein at 12 h. KC levels in the skin of mice challenged with either WT or the Δ*scpA* mutant did not increase significantly and remained 6- to 13-fold lower than the corresponding levels measured for the double mutant (Figure 4A). Skin levels of MIP-2 exhibited a similar behavior, peaking at 9 ng/mg of extracted protein for Δ*scpA*/Δ*scpC*-infected mice, and showing 2- to 4.8-fold lower quantities for animals challenged with either the WT or the Δ*scpA* mutant (Figure 4B). In contrast, mice challenged with either the WT or the mutants had similar skin levels of LIX, peaking at 3.5 ng/mg of extracted protein (Figure 4C). The deferential ability of ScpC to degrade KC, MIP-2, and LIX *in vivo*, as reflected in the results of Figure 4A–C, respectively, is in agreement with the cleavage specificity of ScpC as determined *in vitro* (Figure 3E). In contrast to the deferential degradation of KC and MIP-2 in the skin, the levels of these chemokines in spleens (Figure 4D and E) and sera (Figure 4F and G) from all three groups of mice did not differ significantly. These findings demonstrate that GAS ScpC acts locally in the infected skin.

To ascertain that the WT, the Δ*scpA*, and the Δ*scpA*/Δ*scpC* mutants triggered similar immune responses in the murine infected skin, we quantified the mRNA levels of KC, IL-6, and IL-1β by real-time RT–PCR. The corresponding mRNA levels (normalized to that of β-actin) were considerably induced in challenged animals compared to animals injected with PBS alone, reaching similar levels in the three groups of mice (Supplementary Figure 5S).

MIP-2 and KC, which were degraded both *in vitro* (Figure 3) and *in vivo* (Figure 4), were the most effective CXC chemokines in mobilizing murine PMNs, as determined in migration assays of isolated PMNs from mouse bone marrow (Supplementary Figure 6S). Neither LIX_{93} nor LIX_{74} induced a significant chemotactic activity at a concentration of 100 ng/ml, under which both MIP-2 and KC fully stimulated PMN migration (Supplementary Figure 6S).

We assessed myeloperoxidase (MPO) activity, which is a well-established marker for PMN activity (Hansson *et al*, 2006), and wound histopathology in mice infected with the isogenic GAS strains. Homogenates of skin lesions produced by either the WT GAS or the Δ*scpA* mutant strains possessed significantly less (at least 3.5-fold) MPO activity than homogenates from skin lesions of mice challenged with the Δ*scpA*/Δ*scpC* mutant (Figure 5A). To demonstrate that the PMN response is local, we challenged mice with the WT and the

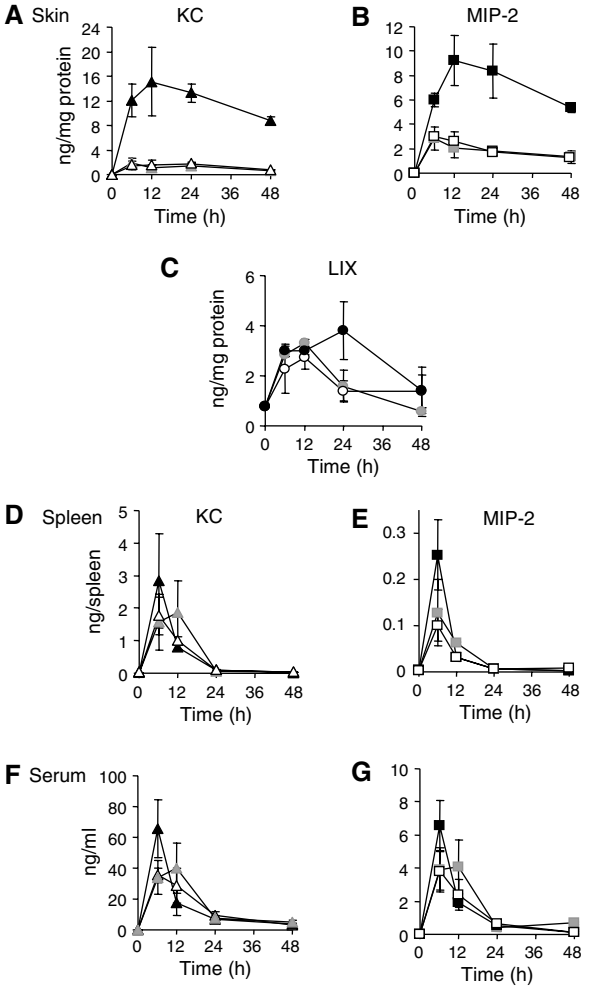

Figure 4 ScpC is responsible for degradation of KC and MIP-2 in infected skin. (**A**) KC levels (ng/mg protein) extracted from skin lesions of mice inoculated with WT (△), Δ*scpA* (△), and Δ*scpA*/Δ*scpC* (▲). Each point represents mean of the determinations performed on three mice killed at the indicated time points after infection. Assays by ELISA were conducted in duplicate. Error bars represent s.d. $P<0.05$ (Student's test) of Δ*scpA*/Δ*scpC* versus WT or versus Δ*scpA* for each time point. $P>0.05$ (Student's test) for WT versus Δ*scpA*. (**B**) MIP-2 levels (ng/mg protein) extracted from skin lesions of mice inoculated with WT (□), Δ*scpA* (□), and Δ*scpA*/Δ*scpC* (■). Each point represents mean of the determinations performed on three mice killed at the indicated time points after infection. Assays by ELISA were conducted in duplicate. Error bars represent s.d. $P<0.01$ (Student's test) of Δ*scpA*/Δ*scpC* versus WT or versus Δ*scpA*. $P>0.05$ (Student's test) for WT versus Δ*scpA* for each time point. (**C**) LIX levels (ng/mg protein) extracted from skin lesions of mice inoculated with WT (○), Δ*scpA* (○), and Δ*scpA*/Δ*scpC* (●). Each point represents mean of the determinations performed on three mice killed at the indicated time points after infection. Assays by ELISA were conducted in duplicate. Error bars represent s.d. $P>0.05$ (Student's test) of Δ*scpA*/Δ*scpC* versus WT or versus Δ*scpA*. $P>0.05$ (Student's test) for WT versus Δ*scpA* for each time point. (**D**) KC levels (ng/spleen) in spleens of three mice from the same groups of mice described in panel A. Assays by ELISA were conducted in duplicate. Error bars represent s.d. $P>0.05$ (Student's test) of Δ*scpA*/Δ*scpC* versus WT or versus Δ*scpA* for each time point. (**E**) MIP-2 levels (ng/spleen) in spleens of three mice from the same groups of mice described in panel B. Assays by ELISA were conducted in duplicate. Error bars represent s.d. $P>0.05$ (Student's test) of Δ*scpA*/Δ*scpC* versus WT or versus Δ*scpA* for each time point. (**F**) KC levels (ng/ml) in sera of three mice from the same groups of mice described in panel A. Assays by ELISA were conducted in duplicate. Error bars represent s.d. $P>0.05$ (Student's test) of Δ*scpA*/Δ*scpC* versus WT or versus Δ*scpA* for each time point. (**G**) MIP-2 levels (ng/ml) in sera of three mice from the same groups of mice described in panel B. Assays by ELISA were conducted in duplicate. Error bars represent s.d. $P>0.05$ (Student's test) of Δ*scpA*/Δ*scpC* versus WT or versus Δ*scpA* for each time point.

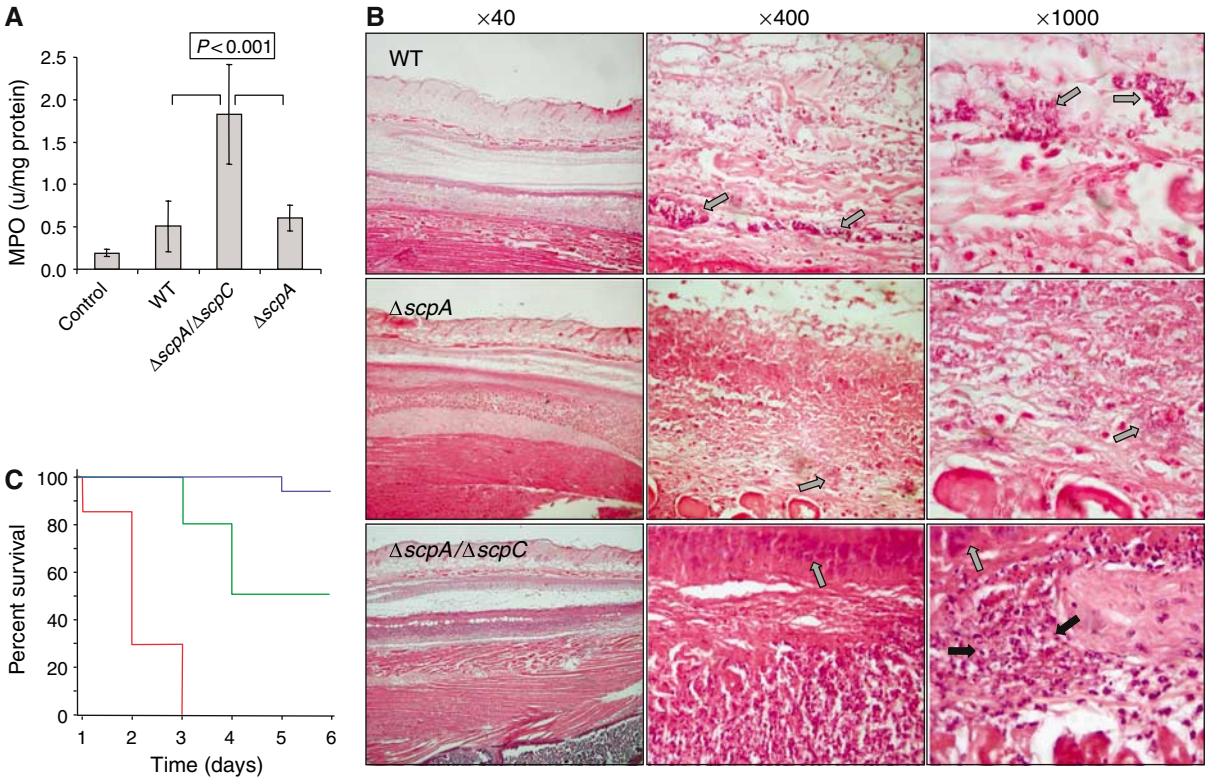

Figure 5 ScpC impairs PMN recruitment. (**A**) Forty-eight hours after inoculation, lesional (GAS) and control (PBS) 6 mm punch biopsy specimens were taken and the amount of MPO activity (units/mg protein) was determined. Each bar represents the mean ± s.d. of two determinations conducted on four specimens. $P<0.001$ (Student's test) of Δ*scpA*/Δ*scpC* versus either WT or Δ*scpA*. (**B**) Representative photomicrographs of sections labeled with H&E prepared 2 days after inoculation with WT and its derived mutants. The gray arrow indicates presence of bacteria whereas the black arrow indicates presence of PMN. (**C**) PMN depletion renders mice sensitive to the Δ*scpA*/Δ*scpC* mutant. Mice were injected subcutaneously with 1×10^8 CFU of Δ*scpA*/Δ*scpC* and survival was monitored daily in cyclophosphamide-treated (— $n=7$), RB6-8C5-treated (— $n=10$), or PBS-treated (— $n=17$) mice. The Kaplan–Meier analysis shows statistically significant difference ($P<0.001$) in the survival of the three groups of mice (using the log rank (Mantel–Cox) test).

Δ*scpA*/Δ*scpC* mutant by injecting the same mouse at opposite flanks with each of the bacterial strains. After 48 h, we found that the MPO activity in the lesions created by the WT was significantly lower (by 2.3-fold) than that in the lesions created by the Δ*scpA*/Δ*scpC* mutant (Supplementary Figure 7Sa). An opposite relationship was observed for the lesion size and its macroscopic appearance (Supplementary Figure 7Sb).

Sections of epidermis, dermis, adipose-panniculus, subcutaneous fat-connective tissue, and skeletal muscle were examined histologically. Twenty-four hours after inoculation, with any of the three GAS strains, mice displayed a focal necrosis of the epidermis and dermis-panniculus with some edema. In subcutaneous fat-connective tissue, we observed focal necrosis, cell debris, many GAS bacteria, and some PMN infiltration. PMN infiltration was more pronounced in animals infected with the Δ*scpA*/Δ*scpC* mutant. No significant differences in skeletal muscle histology were observed among the three groups, with all mice showing superficial edema. Two days after inoculation, histological differences between the groups were evident. Extensive necrosis, vascular degeneration, bacterial spread, and a paucity or complete absence of PMNs were observed in the subcutaneous fat-connective tissue and skeletal muscles of mice challenged with either the WT or the Δ*scpA* mutant strains (Figure 5B). In comparison, tissue sections of mice inoculated with the Δ*scpA*/Δ*scpC* mutant exhibited necrosis and showed bacterial presence but revealed a marked PMN infiltration (Figure 5B).

To confirm that PMN infiltration plays a major role in rendering mice resistant to the infection by Δ*scpA*/Δ*scpC* mutant, we tested the virulence of the Δ*scpA*/Δ*scpC* mutant in PMN-depleted mice. PMN depletion was achieved by intraperitoneal injection of mice with either cyclophosphamide or the anti-GR1 antibody (RB6-8C5). Depletion of PMNs by both means rendered mice sensitive to the double mutant as compared to control mice, which were completely resistant (Figure 5C). The cyclophosphamide-treated mice were more sensitive than the RB6-8C5-treated mice, probably because the drug reduces also the populations of lymphocytes and monocytes (Braff *et al*, 2005). In conclusion, ScpC through its ability to degrade CXC chemokines impairs PMN recruitment to the site of infection, facilitating GAS survival and systemic spread.

Discussion

GAS NF is characterized by extensive local necrosis of subcutaneous soft tissues and skin and its microbiologic etiology is confirmed by isolation of the pathogen from a normally sterile body site. Because of the rapid progression of necrosis in GAS NF patients, medical treatment typically includes extensive debridement of soft tissues and occasionally neces-

sitates amputation of extremities. Consequently, GAS has been coined by the public as 'the flesh-eating bacterium'.

Impairment of PMN recruitment plays a central role in the pathogenesis of NF. A recent review of histopathological analysis of soft tissues debrided from human NF patients with highest disease severity revealed very few or absence of PMNs at the infection site (Bakleh *et al*, 2005). In the baboon model of human NF, surviving baboons have an intense PMN influx into the site of inoculation, whereas those that die have no PMN influx at all (Taylor *et al*, 1999). In our previous studies, we show that mice challenged with the WT GAS M14 strain develop a lethal infection that is typified by the absence of PMN migration to the initial site of infection, mirroring the pathological findings in the NF patient from which the bacterium was first isolated (Hidalgo-Grass *et al*, 2004). There, PMN infiltration was absent in necrotic tissues with high bacterial load but was clearly apparent in the non-necrotic surrounding tissues that were free of bacteria (Hidalgo-Grass *et al*, 2004). Thus, inhibition of PMN recruitment by GAS may be a local phenomenon evident only in the immediate vicinity of invading bacteria.

In this study, we used targeted mutagenesis to demonstrate that ScpC (also known as SpyCEP) is the GAS peptidase responsible for proteolysis of both human (IL-8) and the mouse (KC and MIP-2) CXC PMN chemokines. N- and C-terminal truncated LIX have been suggested to act as functional homologs of IL-8 in the mouse (Wuyts *et al*, 1999). LIX is a poor substrate of ScpC, as revealed by *in vitro* assays of degradation and by measuring LIX content in GAS-infected murine skin. Even so, LIX contribution to murine PMN recruitment seems to be negligible compared to that of MIP-2 or KC, as assessed in assays of PMN migration.

We show that IL-8 is not further degraded beyond its cleavage into two fragments, even following prolonged incubation with WT GAS culture supernatant. This strongly suggests that ScpC is solely responsible for inactivation of the host CXC chemokines. Indeed, it was reported that both IL-8 and MIP-2 are cleaved by partially purified ScpC at analogous positions, between Gln59 and Arg60 and Gln60 and Lys61, respectively (Edwards *et al*, 2005).

scpC transcription is negatively regulated by the SilCR CSP peptide in the M14 strain and this requires the SilA/B TCS. Blood isolates of GAS were better able to degrade human IL-8 than throat isolates, suggesting that ScpC expression is upregulated in invasive GAS isolates (Edwards *et al*, 2005). It would be interesting to decipher the mode of *scpC* regulation in these isolates, particularly in the highly invasive M1 and M3 serotype strains that lack the *sil* locus.

Here, we provide the first evidence that ScpC is an essential GAS virulence factor in the pathogenesis of invasive skin and soft tissue infection. This is best established by the innocuous phenotype of Δ*scpA*/Δ*scpC* mutant (compared to lethal phenotype of the WT) in untreated mice, in contrast to its lethal phenotype in PMN-depleted mice. The GAS C5a peptidase (ScpA) could also be speculated to interfere with PMN recruitment through inactivation of the chemotactic component C5a of the complement system (Wexler *et al*, 1985). However, our finding that ScpA does not contribute to GAS virulence in the murine NF model may reflect the observation that a homolog of ScpA, in *Streptococcus agalactiae*, has far lower activity against murine C5a than the human C5a (Bohnsack *et al*, 1993). ScpA has also been shown to have no effect on mortality in a mouse air sac model (Ji *et al*, 1996).

In summary, we provide the first direct *in vivo* evidence of a novel bacterial virulence mechanism: degradation of host CXC chemokines to prevent PMN recruitment with consequent systemic bacterial spread from the initial tissue focus of infection. The peptidase responsible for this virulence phenotype, ScpC, is highly conserved among all eight available genomes of GAS. Therapies to neutralize ScpC activity or to block its expression (e.g. through administration of SilCR CSP (Hidalgo-Grass *et al*, 2004) and see also Supplementary Figure 1Sb) can represent a novel strategy to enhance the host innate immune response to invasive GAS infection.

Materials and methods

Bacterial strains, growth conditions, and plasmids

Primers, bacterial strains, and plasmids used in the study are described in Supplementary Tables I and II. All experiments and strain construction employed GAS strain JS95 of M14 serotype (Hidalgo-Grass *et al*, 2002; Moses *et al*, 2003). Molecular cloning experiments utilized *Escherichia coli* JM109 strain, which was cultured in Laria-Bertani broth, Lennox (Becton, Dickinson, Sparks, MD, USA). For culturing of GAS, we employed Todd-Hewitt medium (Becton, Dickinson) supplemented with 0.2% yeast extract (Becton, Dickinson) (THY media) with incubation at 37°C in sealed tubes without agitation. To produce solid media, Bacto™ Agar (Becton, Dickinson) was added to a final concentration of 1.4%. Antibiotics were added at the following concentrations when necessary: for GAS: 250 μg/ml kanamycin (Km), 50 μg/ml spectinomycin (Spec), 1 μg/ml erythromycin (Erm), and 7 μg/ml chloramphenicol (Cm); for *E. coli*: 100 μg/ml ampicillin (Amp), 50 μg/ml Spec, 750 μg/ml Erm, and 10 μg/ml Cm. All the antibiotics were purchased from Sigma-Aldrich (St Louis, MO, USA).

Manipulation of DNA

Plasmid DNA was isolated by mini-preps (Roche Applied Science, Basel, Switzerland) or midi-preps (Promega, Madison, WI, USA) according to the manufacturer's instructions and used to transform *E. coli* by standard methods and to transform GAS by electroporation as described previously (Caparon and Scott, 1991). Restriction endonucleases, ligases, and polymerases were used according to the recommendations of the manufacturers. Chromosomal DNA was purified from GAS as described previously (Caparon and Scott, 1991) or by using the Wizard® Genomic DNA Purification Kit (Promega). Linear DNA fragments were purified using Certified™ low-melt agarose (Bio-Rad, Hercules, CA, USA) before electroporation into GAS strains. PCR products were purified using a commercial kit (QIAquick PCR Purification Kit, Qiagen, Hilden, Germany). All other procedures were conducted according to standard protocols (Sambrock and Maniatis, 1989).

RNA isolation and real-time RT–PCR

For RNA preparations, WT or derivative mutants were grown in THY in the absence or presence of SilCR (10 μg/ml) to an OD_{600} of ~0.4. SilCR was synthesized and purified to 96% purity by BioSight (Karmiel, Israel). RNA was prepared by hot acidic phenol extraction as described previously (Ravins *et al*, 2000). Representative samples were assessed for RNA integrity by electrophoretic analysis and measurement of the A_{260}/A_{280} ratio was used to determine the RNA concentration and purity (accepted if >1.8). Contaminating DNA was removed by DNase treatments according to the manufacturer's instructions (RQ1 RNase free DNase, Promega). Samples were rejected if PCR amplification preformed with RNA templates (primers V-*sra*-f and V-*sra*-r; Supplementary Table I) indicated the presence of contaminating DNA. Total RNA (5 μg) was used for cDNA synthesis using M-MLV reverse transcriptase (Promega), according to the manufacturer's protocol. For real-time RT–PCR, primers (Supplementary Table I) were designed using Primer Express™ software v2.0 (Applied Biosystems, Foster City, CA). SYBR-green mix (Applied Biosystems) was used for fluorescence detection with the ABI Prism 7000 SDS real-time PCR system (Applied Biosystems) according to the manufacturer's protocol. The

level of transcription of gyrase subunit A (*gyrA*) was used to normalize expression data for each target gene. Transcription of *gyrA* is constant under a variety of *in vitro* experimental conditions (Graham *et al*, 2002). Each assay was performed in duplicate with at least three RNA templates prepared from bacteria from independent cultures on different days. The data were analyzed according to the standard curve method (Applied Biosystem support) and are presented as abundance of transcript relative to that of *gyrA*. Tissue samples were isolated from lesional (GAS) and control (PBS) mice using 6 mm punch biopsy (Acuderm Inc., USA) 24 h after inoculation. The samples were homogenized by a Polytron (Kinematica AG, Lucerne, Switzerland) in the presence of guanidine thiocyanate and β-mercaptoethanol to prevent degradation by ribonucleases. Total RNA was isolated using SV Total RNA Isolation System (Promega) according to the manufacturer's recommendations. Quantitative real-time PCRs were performed as described above. Primer sequences for *KC*, *IL-6*, *IL-1*β, and the normalizer, β-*actin*, are provided in Supplementary Table I.

Strategy of mutants' construction

Mutant strains of the genotypes *silA*$^-$, Δ*emm*, Δ*scpA*, and Δ*scpA*/Δ*scpC* were derived from strain WT by insertion inactivation or by replacing the corresponding chromosomal genes with either *aad9* or Ω*km2*. Δ*emm* was constructed as described previously (Hidalgo-Grass *et al*, 2002). The deletion mutant Δ*scpA* gene was constructed by replacing 1911 bp of the *scpA* gene with *aad9*. This was carried out by cloning a fragment containing 453 bp of the upstream region of *ScpA*, *aad9*, and 509 bp of the 3′ region of *ScpA*. The upstream region contained the intragenic region between *mga* and *ScpA* and 21 bp of the 5′ end of *scpA* and was PCR amplified using the primers M-*scpC*5′-f and M-*scpA*5′-r (Supplementary Table I). *aad9* was PCR amplified using the plasmid pFW11 as a template and the primers M-*aad9Nco*I-f and M-*aad9Pst*I-r (Supplementary Tables I and II). The downstream region of *scpA* was amplified using the primers M-*scpA*3′-f and M-*scpA*3′-r (Supplementary Table I). *aad9* and its upstream and downstream flanking fragments were cloned into the temperature-sensitive *E. coli-streptococcal* shuttle vector pJRS233 yielding the plasmid p*JscpAaad9* (Supplementary Table II). The plasmid was electroporated into WT, and Erm- and Spec-resistant transformants were isolated at the permissive temperature (30°C). Growth of transformants at the non-permissive temperature (37°C) resulted in the integration of the plasmid. For the second recombination event, one of the single recombination mutants was further passaged for 8 days at 30°C without Erm and colonies were replica plated on THY plates containing either Erm or Spec. Growth of transformants in the presence of Spec but not in the presence of Erm indicated that a second recombination event occurred resulting in *scpA* exchange with the *aad9* and excision of pJRS233 yielding the strain Δ*scpA*. The replacement was verified using the primers M-*scpA*5′-f and M-*scpA*3′-r (Supplementary Table I). The loss of C5a peptidase expression was confirmed by dot blot analysis (Supplementary Figure 2S).

To construct the *silA*-disrupted mutant, the internal region of the gene was PCR amplified using the primers M-*silA*-f and M-*silA*-r (Supplementary Table I), cloned into the pJRS233 vector and transformed into WT, and mutants resistant to Erm were isolated. The fidelity of the single integration was verified by two sets of primers: V-*silA*5′-f/V-M13-r and V-M13-f/V-*silB*3′-r (Supplementary Table I).

To construct the double deletion mutant Δ*scpA*/Δ*scpC*, a DNA fragment of 5313 bp containing *scpC*, 326 bp upstream and 42 bp downstream, was PCR amplified with the high-fidelity polymerase Pwo (Roche) using the primers M-*scpC*-f and M-*scpC*-r (Supplementary Table I). Adenine was added to the ends of the PCR product by Klenow polymerase in the presence of dATP and the DNA fragment was then cloned into pGEM-T-easy vector (Promega) according to the manufacturer's instructions to yield p*GscpC* (Supplementary Table II). An *Eco*RV restriction released a 753 bp from within the *scpC* including the serine 617 required for proteolysis (see Figure 1B). The *Eco*RV fragment was replaced with *Sma*I-digested Ω*km2* (2043 bp) derived from pBRΩ*km2* (Perez-Casal *et al*, 1991), yielding the plasmid p*GscpC*Ω*km2* (Supplementary Table II). The fidelity of the construction was verified by sequencing using the primers V-*scpC*-f and V-*scpC*-r (Supplementary Table I). The *scpC*Ω*km2* fragment was released by digestion of p*GscpC*Ω*km2* with *Eco*RI and the linear fragment of 6623 bp was electroporated into Δ*scpA* and transformants were selected for double homologous recombination on plates containing Km and Spec. The fidelity of *scpC* replacement with *scpC*Ω*km2* allele in Δ*scpA*/Δ*scpC* was verified by PCR with the primers V-*scpC*-f and V-*scpC*-r (Supplementary Table II).

For the complementation of Δ*scpA*/Δ*scpC* with *scpC*, the latter was released from p*GscpC* by digestion with *Eco*RI and cloned into pLZ12 (Supplementary Table II), which was digested with the same enzyme and dephosphorylated before ligation. The *E. coli* colonies resistant to Km and Cm were screened for *scpC* presence using the primers V-*scpC*-f and V-*scpC*-r (Supplementary Table I). The plasmid p*LscpC* was electroporated into Δ*scpA*/Δ*scpC* and transformants were selected on plates containing Km and Cm.

Sequence analyses

Serine peptidases of GAS were retrieved from MEROPS database (Rawlings *et al*, 2004) using *Streptococcus pyogenes* as the key word for an organism. Sequences of *scpC* in the GAS genomes were identified by database homology search using BLAST (BLAST with microbial genomes, NCBI) (Altschul *et al*, 1997). The complete aa sequences of ScpC from the various GAS genomes (*S. pyogenes* M1 strain SF370 (Spy0416, NP_268723), M3 strain MGAS315 (SpyM3_0298, NP_664102), M3 SSI-1 (SPs1559, BAC64654), M5 strain MGAS5005 (M5005_Spy0341, AAZ50960), M6 strain MGAS10394 (M6_Spy0367, AAT86502), M18 strain MGAS8232 (spyM18_0464, NP_606696), M28 strain MGAS6180 (M28_Spy0329, AAX71443), and M49 strain M49 591 (SpyoM01000941, ZP_00365806)), CspA from GBS (AAN85092), and PrtS from *Streptococcus thermophilus* (AAG09771) were analyzed and compared by multiple sequence alignment using VNTI (Vector NTI 9.1.0 2004; Invitrogen Corporation, Carlsbad, CA, USA) and ClustalX (Thompson *et al*, 1997). Domains were identified and analyzed using NCBI Conserved Domain Database Search CDD http://www.ncbi.nlm.nih.gov/Structure/cdd/wrpsb.cgi and by Conserved Domain Architecture Retrieval Tool (CDART) http://www.ncbi.nlm.nih.gov/Structure/lexington/lexington.cgi?cmd = rps. Motifs were identified using ProSite (Motif Scan) (Falquet *et al*, 2002) and by Block Search http://blocks.fhcrc.org/blocks/blocks_search.html. We used SignalP 3.0 Server (Bendtsen *et al*, 2004) to predict the presence and location of signal peptide cleavage sites.

Analysis of ScpA expression

To analyze the expression of ScpA on GAS surface, strains were cultured overnight in THY, washed in PBS by repeated centrifugation, and resuspended in PBS to an $OD_{600} \sim 0.8$. Bacterial suspensions were diluted 1:50 and then diluted serially by two-fold and 3 μl was spotted on two membranes of nitrocellulose. After blocking (10% non-fat milk), the membranes were incubated with anti-ScpA (a generous gift from P Cleary, Minnesota, USA and Patrick Trieu-Cuot, Paris, France) diluted (1:1000) or with anti-GAS (Fitzgerald, USA) diluted (1:3000) antibodies for 2 h. Then, the membranes were washed three times with Tris-buffered saline supplemented with 0.03% Tween 20 (TBS-T), followed by 1 h incubation with a secondary goat anti-rabbit IgG HRP-conjugated (Promega) at a dilution of 1:20 000. Membranes were washed four times in TBS-T and incubated for 5 min with chemiluminescent substrate Super Signal® WestPico (Pierce, Rockford, IL, USA) and dots were visualized on X-ray film after 1 min of exposure.

Blood survival, mouse infection assays, and histology

The ability of GAS to survive in non-human blood as well as the murine model soft tissue infection both were performed as detailed previously (Hidalgo-Grass *et al*, 2002, 2004). For histological analysis, skin samples including underlying bone (lumbar area) were analyzed. Central full-thickness specimens were made and fixed in formalin (10%). Two apposing halves were placed in the block to be processed, so that the examined tissue consisted of the central area of the skin sample. Tissues were decalcified for 4 h and placed in formalin, dissected, and embedded in paraffin. Hematoxylin and eosin (H&E) staining was performed on the paraffin-coated sections. All procedures were carried out by Diagnostic Veterinary Pathology Services (PathoVet, Kfar Bilu, Israel). For analysis, we examined the following sections: epidermis, dermis, adipose-panniculus, subcutaneous fat-connective tissue, and skeletal muscle surrounding vertebrae. Measurements of total lesion size (cm^2) were made by analyzing digital photographs (Nikon Coolpix 5700) of mice taken every day between days 1 and 4 after

inoculation and at day 8 for mice inoculated with the Δ*scpA*/Δ*scpC* double mutant. Analysis was performed with the software program 'Image J' (NIH Research Service Branch http://rsbweb.nih.gov/ij/) and a millimeter ruler as a reference. The Institutional Ethics Committee for animal care approved all animal procedures.

Assay of chemokine degradation in vitro

IL-8, KC, and MIP-2 degradation was performed and quantified by ELISA using the Quantikine kit (R&D Systems, Minneapolis, MN, USA) as detailed previously (Hidalgo-Grass *et al*, 2004). To follow the kinetics of IL-8 degradation by SDS–PAGE, the concentration of IL-8 in the proteolysis reaction (Hidalgo-Grass *et al*, 2004) was increased from 1 to 8 μg/ml and the fetal calf serum in the bacterial supernatant was lowered to 0.1% to enable detection of IL-8 on 17.5% SDS–PAGE. Samples of 24 μl from proteolysis reaction were withdrawn after 30 min, 2 h, and 16 h, then 6 μl of 5 × SDS–PAGE sample buffer was added and samples were boiled for 2 min. Samples were subjected to electrophoresis and protein bands were visualized by silver staining (silver stain kit (Bio-Rad)). To follow the kinetics of IL-8, KC, MIP-2, and RANTES degradation, the chemokines were incubated at an initial concentration of 150 ng/ml and samples of 0.1 ml were withdrawn from the reaction at the desired time points. The amount of the relevant chemokine was determined by ELISA (R&D Systems) as described above.

Assay of chemokine degradation in vivo

The WT and its derived mutants Δ*scpA* and Δ*scpA*/Δ*scpC* were grown and prepared for subcutaneous inoculation exactly as for evaluating mice survival in the soft tissue model of human NF (Hidalgo-Grass *et al*, 2002, 2004). At specific times after injection, mice were killed and various tissues were isolated. Tissue sections surrounding the lesion were incised and minced with scissors. The chemokines were extracted from the disrupted tissues by incubation for 1 h at room temperature with lysis buffer containing 10 mM Tris–HCl pH 7.8, supplemented with 1% NP-40, 150 mM NaCl, and 40 mM EDTA. The presence or absence of complete Minimix protease inhibitors (Roche) did not affect the content of the extracted chemokines. The extracts were spun at 17 000 *g* for 5 min at room temperature. The supernatants were stored at −80°C until all samples were collected. The amounts of KC, MIP-2, and LIX were determined by ELISA (R&D Systems) and normalized according to the protein content of the corresponding samples, which was measured by BIO-RAD protein assay (Bio-Rad Laboratories). Isolated spleens were gently disrupted and suspended in Dulbecco's PBS (Sigma), containing complete minimix protease inhibitors (Roche). Supernatants of spleen suspensions were accumulated and the amounts of KC and MIP-2 were determined as described above. Blood samples were obtained by cardiac puncture. After coagulation, sera were collected and the amounts of KC and MIP-2 were determined as described.

MPO assay

Lesional 6 mm punch biopsy (Acuderm) specimens were incised and then homogenized for 30 s at 0°C by Polytron (Kinematica AG, Lucerne, Switzerland). MPO activity was determined with an MPO assay kit according to the manufacturer's recommendations (Cytostore, Calgary, Alberta, Canada). The MPO units of activity were normalized according to the protein content present in the corresponding samples, which was measured by BIO-RAD protein assay (Bio-Rad Laboratories).

Neutrophil isolation and transwell migration assays

Bones from BALB/c mice were splashed with PBS and cells were treated with RBC lysing solution (0.155 M NH_4Cl, 0.01 M $KHCO_3$, 0.01 mM EDTA, pH 7.4), washed, and then re-suspended in RPMI (600 μl) supplemented with 1% FCS. The assay of PMN migration to the indicated concentrations (2, 10, and 100 ng/ml) of KC, MIP-2, LIX_{74}, and LIX_{93} (R&D Systems and Cytolab/Peprotech Asia) was performed as described previously (Beider *et al*, 2003). Briefly, RPMI (600 μl) supplemented with 1% FCS containing the chemokines at the indicated concentrations was placed into the lower chamber of a Costar 24-well transwell (Corning, NY). Cells (2×10^5) in 100 μl medium were placed into the upper chamber (pore size 5 μm) and cells were collected from both chambers after 4 h of migration at 37°C and counted by flow cytometry (FACSsort, Becton Dickinson, San Jose, CA) after labeling with anti-GR1 antibody. Percentage of migrating PMN was calculated by dividing the number of migrating PMNs by the total number of PMNs present.

PMN depletion

PMN depletion was achieved by administration of either cyclophosphamide or the monoclonal antibody RB6-8C5 (R&D) into the BALB/c mice used for the model of human NF, according to the procedure described previously (Braff *et al*, 2005) with the following modifications. Mice were injected with Δ*scpA*/Δ*scpC* mutant 48 h after cyclophosphamide treatment with 3 μg/mouse. After 48 h, the number of circulating PMNs in the peripheral blood dropped from 6% to less than 0.6% as determined by flow cytometry (FACSsort, Becton Dickinson, San Jose, CA), following labeling with anti-GR1 antibody (R&D). The amount of administered monoclonal antibody RB6-8C5 was 0.1 μg/mouse. Twenty-four hours after treatment, the number of circulating PMNs in the peripheral blood dropped from 9 to 2%.

Supplementary data

Supplementary data are available at *The EMBO Journal* Online (http://www.embojournal.org).

Acknowledgements

We thank Pat Cleary (Department of Microbiology, University of Minnesota, Minneapolis, MN, USA) and Patrick Trieu-Cuot (Unit of Gram-positive Bacterial Pathogens, Institute Pasteur, Paris, France) for providing us with the anti-ScpA antibody and Miriam Ravins (Institute of Microbiology, The Hebrew University-Hadassah Medical School) for participating in the construction of the *scpA*-deficient mutant and for critical reading of the manuscript. We thank Hana Wald from the Goldyne Savad Institute of Gene Therapy for technical assistance. We thank Nahum Shpigel for encouragement and for valuable suggestions concerning the MPO assay. This work was supported by grants from the USA–Israel Binational Science Foundation (to EH and VN), the Center for the Study of Emerging Diseases (to EH), and The Israeli Science Foundation administered by the Israel Academy of Science and Humanities (to EH). EH is an international research scholar from the Howard Hughes Medical Institute.

References

Altschul SF, Madden TL, Schaffer AA, Zhang J, Zhang Z, Miller W, Lipman DJ (1997) Gapped BLAST and PSI-BLAST: a new generation of protein database search programs. *Nucleic Acids Res* **25:** 3389–3402

Bakleh M, Wold LE, Mandrekar JN, Harmsen WS, Dimashkieh HH, Baddour LM (2005) Correlation of histopathologic findings with clinical outcome in necrotizing fasciitis. *Clin Infect Dis* **40:** 410–414

Beider K, Nagler A, Wald O, Franitza S, Dagan-Berger M, Wald H, Giladi H, Brocke S, Hanna J, Mandelboim O, Darash-Yahana M, Galun E, Peled A (2003) Involvement of CXCR4 and IL-2 in the homing and retention of human NK and NK T cells to the bone marrow and spleen of NOD/SCID mice. *Blood* **102:** 1951–1958

Bendtsen JD, Nielsen H, von Heijne G, Brunak S (2004) Improved prediction of signal peptides: signalP 3.0. *J Mol Biol* **340:** 783–795

Bisno AL, Brito MO, Collins CM (2003) Molecular basis of group A streptococcal virulence. *Lancet Infect Dis* **3:** 191–200

Bohnsack JF, Chang JK, Hill HR (1993) Restricted ability of group B streptococcal C5a-ase to inactivate C5a prepared from different animal species. *Infect Immun* **61:** 1421–1426

Braff MH, Zaiou M, Fierer J, Nizet V, Gallo RL (2005) Keratinocyte production of cathelicidin provides direct activity against bacterial skin pathogens. *Infect Immun* **73:** 6771–6781

Caparon MG, Scott JR (1991) Genetic manipulation of pathogenic streptococci. *Methods Enzymol* **204:** 556–586

Clark-Lewis I, Schumacher C, Baggiolini M, Moser B (1991) Structure–activity relationships of interleukin-8 determined using chemically synthesized analogs. Critical role of NH2-terminal residues and evidence for uncoupling of neutrophil chemotaxis, exocytosis, and receptor binding activities. *J Biol Chem* **266:** 23128–23134

Claverys JP, Havarstein LS (2002) Extracellular-peptide control of competence for genetic transformation in *Streptococcus pneumoniae*. *Front Biosci* **7:** d1798–d1814

Cleary PP, Kaplan EL, Handley JP, Wlazlo A, Kim MH, Hauser AR, Schlievert PM (1992) Clonal basis for resurgence of serious *Streptococcus pyogenes* disease in the 1980s. *Lancet* **339:** 518–521

Cunningham MW (2000) Pathogenesis of group A streptococcal infections. *Clin Microbiol Rev* **13:** 470–511

Davies HD, McGeer A, Schwartz B, Green K, Cann D, Simor AE, Low DE (1996) Invasive group A streptococcal infections in Ontario, Canada. Ontario Group A Streptococcal Study Group. *N Engl J Med* **335:** 547–554

DeMaster E, Schnitzler N, Cheng Q, Cleary P (2002) M(+) group A streptococci are phagocytized and killed in whole blood by C5a-activated polymorphonuclear leukocytes. *Infect Immun* **70:** 350–359

Edwards RJ, Taylor GW, Ferguson M, Murray S, Rendell N, Wrigley A, Bai Z, Boyle J, Finney SJ, Jones A, Russell HH, Turner C, Cohen J, Faulkner L, Sriskandan S (2005) Specific C-terminal cleavage and inactivation of interleukin-8 by invasive disease isolates of *Streptococcus pyogenes*. *J Infect Dis* **192:** 783–790

Falquet L, Pagni M, Bucher P, Hulo N, Sigrist CJ, Hofmann K, Bairoch A (2002) The PROSITE database, its status in 2002. *Nucleic Acids Res* **30:** 235–238

Gillitzer R, Goebeler M (2001) Chemokines in cutaneous wound healing. *J Leukoc Biol* **69:** 513–521

Graham MR, Smoot LM, Migliaccio CA, Virtaneva K, Sturdevant DE, Porcella SF, Federle MJ, Adams GJ, Scott JR, Musser JM (2002) Virulence control in group A Streptococcus by a two-component gene regulatory system: global expression profiling and *in vivo* infection modeling. *Proc Natl Acad Sci USA* **99:** 13855–13860

Hansson M, Olsson I, Nauseef WM (2006) Biosynthesis, processing, and sorting of human myeloperoxidase. *Arch Biochem Biophys* **445:** 214–224

Hassell M, Fagan P, Carson P, Currie BJ (2004) Streptococcal necrotising fasciitis from diverse strains of *Streptococcus pyogenes* in tropical northern Australia: case series and comparison with the literature. *BMC Infect Dis* **4:** 60

Hidalgo-Grass C, Dan-Goor M, Maly A, Eran Y, Kwinn LA, Nizet V, Ravins M, Jaffe J, Peyser A, Moses AE, Hanski E (2004) Effect of a bacterial pheromone peptide on host chemokine degradation in group A streptococcal necrotising soft-tissue infections. *Lancet* **363:** 696–703

Hidalgo-Grass C, Ravins M, Dan-Goor M, Jaffe J, Moses AE, Hanski E (2002) A locus of group A *Streptococcus* involved in invasive disease and DNA transfer. *Mol Microbiol* **46:** 87–99

Husmann LK, Scott JR, Lindahl G, Stenberg L (1995) Expression of the Arp protein, a member of the M protein family, is not sufficient to inhibit phagocytosis of *Streptococcus pyogenes*. *Infect Immun* **63:** 345–348

Ji Y, McLandsborough L, Kondagunta A, Cleary PP (1996) C5a peptidase alters clearance and trafficking of group A streptococci by infected mice. *Infect Immun* **64:** 503–510

Johnson DR, Wotton JT, Shet A, Kaplan EL (2002) A comparison of group A streptococci from invasive and uncomplicated infections: are virulent clones responsible for serious streptococcal infections? *J Infect Dis* **185:** 1586–1595

Kaul R, McGeer A, Low DE, Green K, Schwartz B (1997) Population-based surveillance for group A streptococcal necrotizing fasciitis: clinical features, prognostic indicators, and microbiologic analysis of seventy-seven cases. Ontario Group A Streptococcal Study. *Am J Med* **103:** 18–24

Miller LS, O'Connell RM, Gutierrez MA, Pietras EM, Shahangian A, Gross CE, Thirumala A, Cheung AL, Cheng G, Modlin RL (2006) MyD88 mediates neutrophil recruitment initiated by IL-1R but not TLR2 activation in immunity against *Staphylococcus aureus*. *Immunity* **24:** 79–91

Monnickendam MA, McEvoy MB, Blake WA, Gaworzewska ET, Hallas G, Tanna A, Efstratiou A, George RC (1997) Necrotising fasciitis associated with invasive group A streptococcal infections in England and Wales. *Adv Exp Med Biol* **418:** 87–89

Morrison DA, Lee MS (2000) Regulation of competence for genetic transformation in *Streptococcus pneumoniae*: a link between quorum sensing and DNA processing genes. *Res Microbiol* **151:** 445–451

Moses AE, Hidalgo-Grass C, Dan-Goor M, Jaffe J, Shetzigovsky I, Ravins M, Korenman Z, Cohen-Poradosu R, Nir-Paz R (2003) emm typing of M nontypeable invasive group A streptococcal isolates in Israel. *J Clin Microbiol* **41:** 4655–4659

O'Brien KL, Beall B, Barrett NL, Cieslak PR, Reingold A, Farley MM, Danila R, Zell ER, Facklam R, Schwartz B, Schuchat A (2002) Epidemiology of invasive group a streptococcus disease in the United States, 1995–1999. *Clin Infect Dis* **35:** 268–276

Perez-Casal J, Caparon MG, Scott JR (1991) Mry, a *trans*-acting positive regulator of the M protein gene of *Streptococcus pyogenes* with similarity to the receptor proteins of two-component regulatory systems. *J Bacteriol* **173:** 2617–2624

Ravins M, Jaffe J, Hanski E, Shetzigovski I, Natanson-Yaron S, Moses AE (2000) Characterization of a mouse-passaged, highly encapsulated variant of group A streptococcus in *in vitro* and *in vivo* studies. *J Infect Dis* **182:** 1702–1711

Rawlings ND, Tolle DP, Barrett AJ (2004) MEROPS: the peptidase database. *Nucleic Acids Res* **32:** D160–D164

Sambrock JFFF, Maniatis T (1989) *Molecular Cloning: A Laboratory Manual*. Cold Spring Harbor, NY: Cold Spring Harbor Press

Sharkawy A, Low DE, Saginur R, Gregson D, Schwartz B, Jessamine P, Green K, McGeer A (2002) Severe group a streptococcal soft-tissue infections in Ontario: 1992–1996. *Clin Infect Dis* **34:** 454–460

Siezen RJ (1999) Multi-domain, cell-envelope proteinases of lactic acid bacteria. *Antonie Van Leeuwenhoek* **76:** 139–155

Taylor Jr FB, Bryant AE, Blick KE, Hack E, Jansen PM, Kosanke SD, Stevens DL (1999) Staging of the baboon response to group A streptococci administered intramuscularly: a descriptive study of the clinical symptoms and clinical chemical response patterns. *Clin Infect Dis* **29:** 167–177

Thompson JD, Gibson TJ, Plewniak F, Jeanmougin F, Higgins DG (1997) The CLUSTAL_X windows interface: flexible strategies for multiple sequence alignment aided by quality analysis tools. *Nucleic Acids Res* **25:** 4876–4882

Ton-That H, Marraffini LA, Schneewind O (2004) Protein sorting to the cell wall envelope of Gram-positive bacteria. *Biochim Biophys Acta* **1694:** 269–278

Wexler DE, Chenoweth DE, Cleary PP (1985) Mechanism of action of the group A streptococcal C5a inactivator. *Proc Natl Acad Sci USA* **82:** 8144–8148

Wuyts A, Govaerts C, Struyf S, Lenaerts JP, Put W, Conings R, Proost P, Van Damme J (1999) Isolation of the CXC chemokines ENA-78, GRO alpha and GRO gamma from tumor cells and leukocytes reveals NH2-terminal heterogeneity. Functional comparison of different natural isoforms. *Eur J Biochem* **260:** 421–429